APS physics

CHORUS

This is the accepted manuscript made available via CHORUS. The article has been published as:

Closed-form tidal approximants for binary neutron star gravitational waveforms constructed from high-resolution numerical relativity simulations

Tim Dietrich, Sebastiano Bernuzzi, and Wolfgang Tichy

Phys. Rev. D **96**, 121501 — Published 7 December 2017

DOI: 10.1103/PhysRevD.96.121501

Closed-form tidal approximants for binary neutron star gravitational waveforms constructed from high-resolution numerical relativity simulations

Tim Dietrich[1], Sebastiano Bernuzzi[2,3], and Wolfgang Tichy[4]
[1]*Max Planck Institute for Gravitational Physics (Albert Einstein Institute), Am Mühlenberg 1, Potsdam 14476, Germany*
[3]*Dipartimento di Scienze Matematiche Fisiche ed Informatiche,*
Universitá di Parma, Parco Area delle Scienze 7/A, I-43124 Parma, Italia
[3]*Istituto Nazionale di Fisica Nucleare, Sezione Milano Bicocca,*
gruppo collegato di Parma, Parco Area delle Scienze 7/A, I-43124 Parma, Italia and
[4]*Department of Physics, Florida Atlantic University, Boca Raton, FL 33431 USA*
(Dated: November 15, 2017)

We construct closed-form gravitational waveforms (GWs) with tidal effects for the coalescence of binary neutron stars. The method relies on a new set of eccentricity-reduced and high-resolution numerical relativity (NR) simulations and is composed of three steps. First, tidal contributions to the GW phase are extracted from the time-domain NR data. Second, those contributions are employed to fix high-order coefficients in an effective and resummed post-Newtonian expression. Third, frequency-domain tidal approximants are built using the stationary phase approximation. Our tidal approximants are valid from the low frequencies to the strong-field regime. They can be analytically added to any binary black hole GW model to obtain a binary neutron star waveform, either in the time or in the frequency domain. This work provides simple, flexible, and accurate models ready to be used in both searches and parameter estimation of binary neutron star events.

PACS numbers: 04.25.D-, 04.30.Db, 95.30.Sf, 95.30.Lz, 97.60.Jd

The 2015 detections of gravitational waves (GWs) of merging binary black holes (BBHs) [1, 2] have initiated a new observational era in astronomy and fundamental physics. In the coming years, ground-based advanced interferometers will reach design sensitivity and observe the coalescence and merger of binary neutron stars (BNSs) [3]. These observations will have a unique potential to probe the fundamental physics of NSs and to connect high-energy astrophysical phenomena with their strong-gravity engines. Main examples are the possibility to constrain the equation of state (EOS) of the cold ultradense matter in NS interiors, e.g. [4], and the possibility to show the unequivocal connection between electromagnetic signals, e.g. short gamma ray bursts [5] or kilonovae [6], with the collision of two compact objects.

A key open problem for GW astronomy with BNS sources is the availability of faithful waveform models that capture the strong-gravity and tidally-dominated regime of the late-inspiral and merger. State-of-art tidal waveform models have been developed in [7, 8] and are based on the effective-one-body (EOB) description of the general-relativistic two body problem [9, 10]. That approach proved to be very powerful but has also limitations. EOB waveforms cannot be efficiently evaluated, hence they cannot be directly used for GW searches or parameter estimation. Fast representations of EOB can be build using reduced-order-modeling techniques [11], but they require extra efforts and introduce further uncertainties. Additionally, the currently published tidal EOB models neither include spin effects nor are tested against spinning NR simulations [12]. Recent work also showed that the current EOB models are not uniformly accurate on the binary parameter space that has been simulated in Ref. [13, 14]. Thus, modeling techniques complementary to EOB, see e.g. [15, 16], are needed especially because post-Newtonian (PN) approximants fail towards merger and introduce systematic uncertainties in GW parameter estimation [17–19].

In this work we construct for the first time closed-form (analytical) approximants to the tidal GW phase directly employing numerical relativity (NR) simulations. Simple time and frequency domain approximants are build from a set of error-controlled BNS merger simulations. Our method is inspired by some ideas used in the modeling of BBH's GWs. In particular, it makes direct use of NR data as in the Phenom approach [20] and employs resummed PN expressions as in the EOB approach.

Eccentricity-reduced and high-resolution NR simulations. For this work we simulated nine BNS configurations in general relativity. We simulated equal-masses BNSs both irrotational and with spins (anti-) aligned to the orbital angular momentum. Three different parameterized EOSs (MS1b, H4, SLy) [21] are employed to span a large range of tidal parameters (see below). The binary gravitational mass is $M = M_A + M_B \sim 2.7$, where A, B label the NSs and M_A is the mass of star A in isolation. Spin magnitudes are in the range $\chi_A = \chi_B \sim [-0.1, +0.15]$, where $\chi_A = S_A/M_A^2$ is the mass-rescaled dimensionless spin. We use the numerical methods implemented in the pseudospectral initial data SGRID code [22] and in the 3+1 adaptive-mesh-refinement evolution BAM code [23]. Key technical points are the use of the Z4c formulation of general relativity and of an high-order scheme for the hydrodynamics [24, 25]. See [26] for further details. Note that we employ geometric units $G = c = M_\odot = 1$.

These new simulations significantly improve the

waveform's quality over previous ones. Low-eccentricity initial data were generated following Ref. [27]; our BNSs have $e \sim 10^{-3}$. Each BNS is evolved using four to five grid resolutions making a total of 37 runs. The NSs are resolved with smallest grid spacings in the range $dx = 0.291 - 0.059$ in each direction. These are the largest BNS simulations performed with the BAM code so far and utilized $\sim$ 25 million CPU hours on various high-performance-computing clusters. Numerical uncertainties are estimated from convergence tests and a detailed error budget has been computed. Our waveforms have maximal errors at merger, accumulated over ~ 12 orbits, of $\sim 0.5 - 1.5$ radians, depending on the particular configuration [26].

Extraction of tidal contributions. Spin and tidal effects in the phase of the complex GW $h(t) = A(t)\mathrm{e}^{-\mathrm{i}\phi(t)}$ are parametrized to leading PN order respectively by the effective spin

$$\chi_{\rm eff} = X_A\chi_A + X_B\chi_B - \frac{38}{113}X_AX_B(\chi_A + \chi_B) \qquad (1)$$

describing the spin-orbit (SO) interaction [28], and by an effective tidal coupling constant [10, 30]

$$\kappa^T_{\rm eff} = \frac{2}{13}\left[\left(1 + 12\frac{X_B}{X_A}\right)\left(\frac{X_A}{C_A}\right)^5 k^A_2 + (A \leftrightarrow B)\right] , \qquad (2)$$

where k^A_2 is the quadrupolar Love number describing the static quadrupolar deformation of one body in the gravitoelectric field of the companion, $X_A = M_A/M$, and C_A is the compactness of star A. $\kappa^T_{\rm eff}$ is defined here for the first time but it based on the expressions for generic mass ratio phasing in [30]. For equal mass systems $\kappa^T_{\rm eff}$ is identical to the dimensionless tidal coupling constant κ^T_2 defined in [10, 34].

In order to separate the tidal phase we work with the phase as a function of the dimensionless GW frequency $\hat{\omega} = M\partial_t\phi(t)$ and use the PN *ansatz*

$$\phi(\hat{\omega}) \approx \phi_0(\hat{\omega}) + \phi_{SO}(\hat{\omega}) + \phi_T(\hat{\omega}) , \qquad (3)$$

where ϕ_0 denotes the nonspinning black hole (or point particle) phase evolution. The SO contribution is $\phi_{\rm SO} \propto \chi_{\rm eff}$ at leading 1.5PN order and it is currently known up to 3.5PN order. For simplicity, we neglect spin-spin interactions; they are subdominant contributions and poorly resolved in our simulations [29]. Tidal contributions enter the phasing at 5PN. The currently known next-to-leading order PN expression of the tidal contribution (TaylorT2 approximant) [19] reads

$$\phi^{\rm T2}_T = -\kappa^T_{\rm eff}\frac{c_{\rm Newt}x^{5/2}}{X_AX_B}(1 + c_1x) , \qquad (4)$$

with $x(\hat{\omega}) = (\hat{\omega}/2)^{2/3}$, where $\hat{\omega}/2$ is the orbital frequency, and $c_{\rm Newt} = -13/8$, $c_1 = 1817/364$ (value for equal mass case). Using Eq. (3) the nonperturbative SO and tidal contributions can be extracted by linearly combining pairs of simulation data with different parameters, as detailed in [12, 26, 29]. The top of Fig. 1 shows the total phase accumulated over simulations. The bottom shows the phase differences divided by the differences in $\kappa^T_{\rm eff}$ for several simulation pairs [26], denoted by $\Delta\phi_T/\Delta\kappa^T_{\rm eff}$. According to Eqs. (3) and (4) $\Delta\phi_T/\Delta\kappa^T_{\rm eff} \approx \phi_T/\kappa^T_{\rm eff}$. For comparison we also show $\phi_T/\kappa^T_{\rm eff}$ of our fit and of TaylorT2. We find that the leading order EOS effect is captured well by $\kappa^T_{\rm eff}$ and the residual dependency on the EOS, related to multipolar tidal coefficients with $\ell > 2$, is negligible. Most importantly, tidal interactions decouple from spin interactions for the spin values explored by NR data and at level of the NR uncertainties. This fact allows us to construct spinning BNSs using binary black hole baseline waveforms and adding the tidal contribution. Further, Fig. 1 indicates that the TaylorT2 approximant does *not* capture the phase evolution in the strong field region, failing for $\hat{\omega} \gtrsim 0.06$, which is approximately the contact frequency [17].

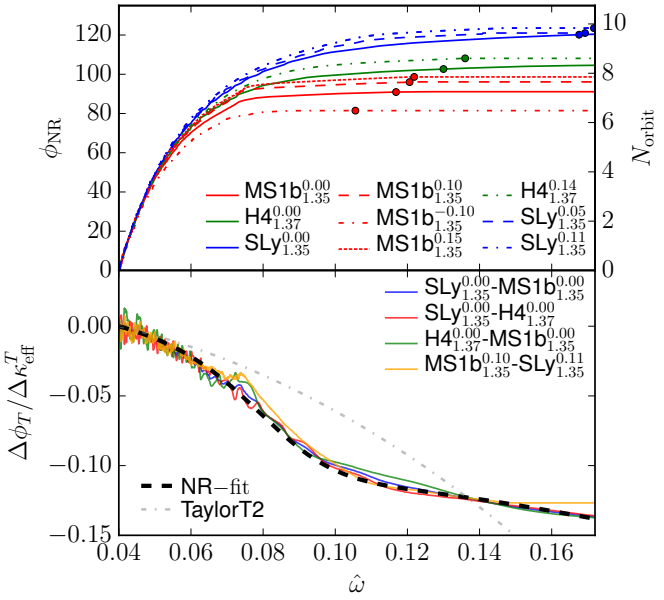

FIG. 1. Phase as a function of the GW frequency from NR simulations. The simulations are labeled as EOS$^{\chi_A}_{M_A}$. Top: Total phase / number of cycles accumulated within frequency interval $\hat{\omega} \in [0.04, 0.17]$ for different BNSs. Markers indicate the merger (peak of the GW's amplitude) of the particular simulation for the highest revolved simulation. Bottom: Pairwise phase differences equivalent to the tidal phase $\phi_T/\kappa^T_{\rm eff}$; note the spin independence.

Time-domain tidal approximant. A closed-form expression for ϕ_T is obtained using the fitting formula

$$\phi_T = -\kappa^T_{\rm eff}\frac{c_{\rm Newt}}{X_AX_B}x^{5/2} \times \frac{1 + n_1x + n_{3/2}x^{3/2} + n_2x^2 + n_{5/2}x^{5/2} + n_3x^3}{1 + d_1x + d_{3/2}x^{3/2}} \qquad (5)$$

Demanding that Eq. (5) reproduces Eq. (4) in a low frequency expansion, we set $d_1 = (n_1 - c_1)$. The other

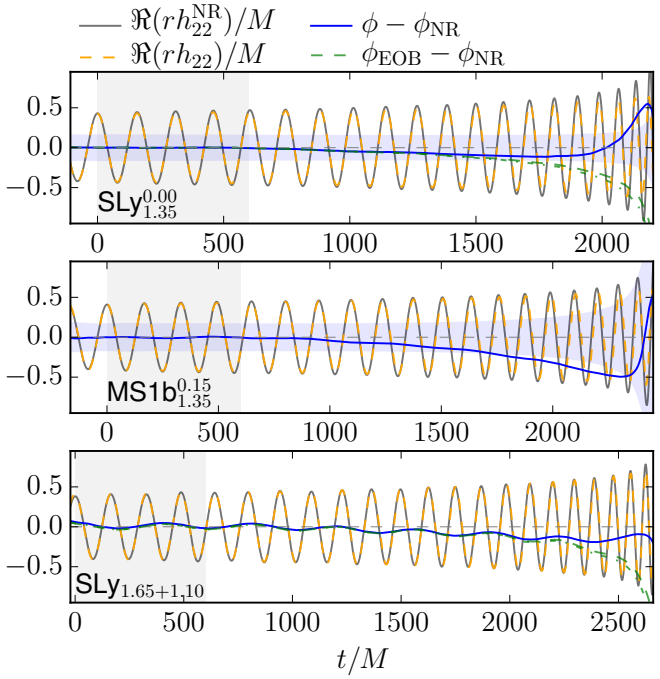

FIG. 2. Comparison of NR simulations with model waveforms obtained following Eq. (3). The panels show the real part of the GW signals (NR data – gray, tidal approximant – orange). We also include the phase between the NR data with respect to our tidal approximant Eq. (5), to Taylor T2 tidal approximant Eq. (4) (cyan), and for some cases to EOB (green dashed [8], green dot dashed [7]. We also indicate the estimated uncertainty of the NR data (blue shaded) and the alignment region (gray shaded). Simulations use the same notation as in Fig. 1 except for the unequal mass case of [14] with EOS$_{M_A+M_B}$.

coefficients are fit to NR data. Note that for simplicity Eq. (5) does not contain tidal terms corresponding to higher multipoles [30], and the dependency from $X_{A,B}$ of the higher effective PN terms is ignored. This is justified since we seek an effective expression of the phase; the coefficients of the latter could be further improved using more simulations with various mass ratios.

The fit is performed on a dataset spanning the interval $\hat{\omega} \in [0, 0.17]$. Eq. (4) is used for $\hat{\omega} \leq 0.0074$, while the tidal EOB waveforms of [7] are used for $\hat{\omega} \geq \in [0.0074, 0.04]$. The datasets are connected such that phase differences near the interval boundaries are minimal. We interpolate the data on a grid consisting of 10000, 5000, 500 points in the three intervals, respectively. Although the final fit depends only weakly on the exact number of points of the interpolating grid, using more points at lower frequencies helps constraining the fit in that regime. Our approximant is defined by Eq. (5) with the fitting coefficients $(n_1, n_{3/2}, n_2, n_{5/2}, n_3) =$ (-17.941,57.983,-298.876,964.192,-936.844), and $d_{3/2} =$ 43.446.

A time-domain approximant of a BNS configuration is computed by prescribing $\kappa^T_{\rm eff}$ and adding Eq. (5) to a BBH baseline, i.e. to ϕ_0. To construct a generic spin-aligned BNS configurations with spin $\chi_{\rm eff}$ we use a BBH waveform that includes already the spin contribution, i.e. use as baseline the GW phase of a BBH setup which has the same dimensionless spin as the BNS configuration which we are going to model. The time-domain phasing is then calculated by numerically integrating $t = \int {\rm d}\phi/\hat{\omega}(\phi)$ in order to obtain a parametric representation of the tidal phase. We stop the integration once $\phi(\hat{\omega})$ reaches its maximum.

Examples of such constructed waveforms are reported in Fig. 2. There, we use the nonspinning BBH waveforms from the SXS-database [31, 32], in particular setup 66 for the equal mass cases and setup 7 for the $q = X_A/X_B = 1.5$ configuration. In order to compare with the BNS configuration with $\chi_{\rm eff} = +0.123$ we add to the nonspinning NR BBH curve the spin-orbit contributions given in Eq. (417) of [28]. In general a spinning binary black hole baseline should be used.

In most cases our new waveforms are compatible with the NR data within the estimated uncertainties. The proposed tidal approximant remains accurate also for longer waveforms. Phase differences with respect to hybrid tidal EOB-NR waveforms and accumulated over the last 300 orbits before merger are of the order of ~ 1 rad, see [26]. In the nonspinning cases, our results can be directly compared to the tidal EOB waveforms of [7, 8] [see green lines in Fig. 2]; comparable performances are observed in spite of the simplicity of our model. The fit gives a good prediction also for the unequal mass case, although only the leading order effect of the mass-ratio is taken into account, see Eq. (2). Also, while we use NR data up to $\hat{\omega} = 0.17$, the model remains accurate for BNSs with smaller $\kappa^T_{\rm eff}$ that merge at higher frequencies. Let us stress that the model performances are independent of the BBH baseline, provided the latter is a faithful representation of BBH waveforms.

Frequency-domain tidal approximant. In the frequency domain $\tilde{h}(f) = f^{-7/6}\tilde{A}(f){\rm e}^{-{\rm i}\Psi(f)}$. The expression of the tidal phase is computed using the stationary phase approximation (SPA) [30]

$$\frac{d^2\Psi_T^{\rm SPA}}{d\omega_f^2} = \frac{Q_\omega(\omega_f)}{\omega_f^2} \ , \tag{6}$$

where ω_f is the Fourier domain circular frequency $\omega_f = 2\pi M f$, and $Q_\omega(\omega) = d\phi/d\log\omega$. The integration of Eq. (6) with (5) is performed numerically; the constants of integration are fixed by demanding continuity with the TaylorF2$_{\rm 1PN}$ in the limit $f \to 0$. The resulting expression $\Psi_T^{\rm NR}$ can be approximated by a Padé function:

$$\Psi_T^{\rm NRP} = -\kappa^T_{\rm eff}\frac{\tilde{c}_{\rm Newt}}{X_A X_B}x^{5/2} \times \frac{1 + \tilde{n}_1 x + \tilde{n}_{3/2}x^{3/2} + \tilde{n}_2 x^2 + \tilde{n}_{5/2}x^{5/2}}{1 + \tilde{d}_1 x + \tilde{d}_{3/2}x^{3/2}} \tag{7}$$

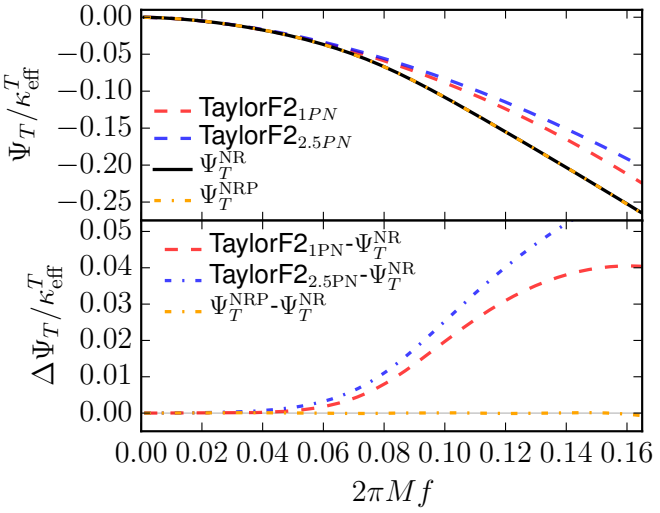

FIG. 3. Frequency-domain tidal approximants. Top panel shows $\Psi_T/\kappa^T_{\rm eff}$ as given by the TaylorF2$_{\rm 1PN}$, TaylorF2$_{\rm 2.5PN}$ [30], Eq. (6), and Eq. (7). Bottom panel: Difference between the frequency-domain representations.

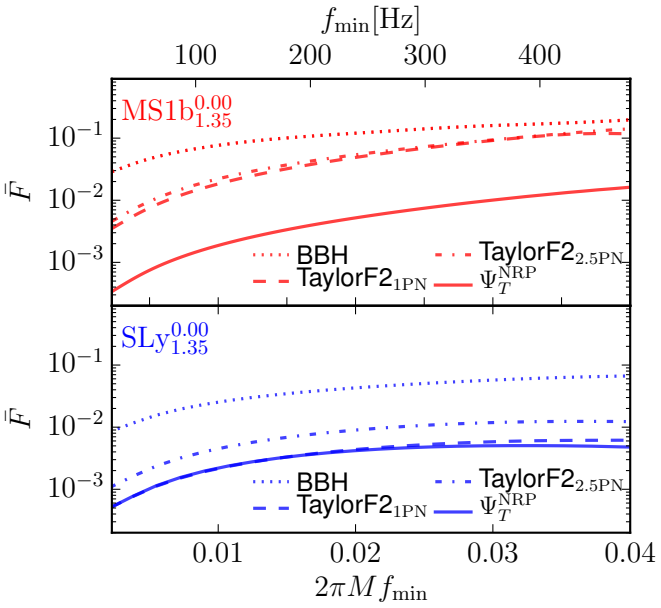

FIG. 4. Unfaithfulness of different approximants with respect to hybridized EOB-NR waveforms for MS1b$^{0.00}_{1.35}$ (top) and SLy$^{0.00}_{1.35}$ (bottom). The unfaithfulness is computed within the interval $M[f_{\rm min}, f_{\rm max}] \sim [0.0022, 0.04]/2\pi$, i.e. $f_{\rm min}$ varies between 27 and 480 Hz. $f_{\rm max}$ is set to the merger frequency of the highest resolved simulation (1398 Hz for MS1b$^{0.00}_{1.35}$ and 2005 Hz for SLy$^{0.00}_{1.35}$). As BBH baseline for $\Psi^{\rm NRP}_T$ we use a nonspinning equal-mass EOB waveform [33].

with $\tilde{c}_{\rm Newt} = 39/16$ and $\tilde{d}_1 = \tilde{n}_1 - 3115/1248$, the other parameters read: $(\tilde{n}_1, \tilde{n}_{3/2}, \tilde{n}_2, \tilde{n}_{5/2})$ = (-17.428,31.867,-26.414,62.362) and $\tilde{d}_{3/2} = 36.089$.

Figure 3 compares the obtained tidal approximants $\Psi^{\rm NR}_T$, $\Psi^{\rm NRP}_T$ with the TaylorF2$_{\rm 1PN}$ and the 2.5PN approximants given in [30] (TaylorF2$_{\rm 2.5PN}$). Because of the construction of Eq. (7) the low frequency behavior of TaylorF2 is recovered. At higher frequencies PN expressions predict smaller tidal effects than $\Psi^{\rm NR}_T$. Considering the accuracy of $\Psi^{\rm NRP}_T$, the Padé fit recovers $\Psi^{\rm NR}_T$ with fractional errors $\lesssim 1\%$.

To further test the performance of the proposed frequency-domain model we compute the unfaithfulness ($\bar{F} = 1 - F$, one minus faithfulness) which is the mismatch for the fixed intrinsic binary parameters with respect to tidal EOB waveforms starting at $\sim$ 25Hz and hybridized with NR simulations [26]. The unfaithfulness quantifies the loss in the signal-to-noise ratio (squared) due to the inaccuracies in the signal modeling. The typical maximum value used in the GW searches is $\bar{F} \leq 0.03$, which roughly corresponds to $\lesssim 10\%$ loss in the number of events (assuming that they are uniformly distributed).

Figure 4 shows $\bar{F}$ for different approximants and varying the minimum frequency in the overlap interval from $Mf_{\rm min} \sim [0.0022, 0.04]/2\pi$, i.e. from $\sim$ 27 Hz to the NR regime ($\sim$ 480 Hz). Tidal approximants have significant mismatches with respect to BBH ones already for $Mf_{\rm min} \sim 0.01/2\pi$. The unfaithfulness computed from $Mf_{\rm min} \sim 0.0022/2\pi$ up to the merger is only weakly dependent on the particular tidal approximant. However, tidal effects become significant at higher frequencies, and if the $\bar{F}$ computations are restricted to higher frequencies significant differences amongst the approximants emerge. $\Psi^{\rm NRP}_T$ has the smallest unfaithfulness. For MS1b$^{0.00}_{1.35}$ (top panel), in particular, the proposed tidal approximant has an unfaithfulness about one order of magnitude smaller than TaylorF2. For SLy$^{0.00}_{1.35}$ (bottom panel) the unfaithfulness is $\bar{F} < 0.03$ for all tidal approximants, indicating that the largest contribution due to tidal effects comes from the strong-field–NR regime.

Conclusion. The tidal approximants proposed here can be efficiently used for both GW searches and parameter estimation of BNS events. For data-analysis applications it is trivial to re-parametrize the tidal coupling constant $\kappa^T_{\rm eff}$ in terms of the mass ratio and (combinations of) the dimensionless tidal parameters that are shown to be optimal for those purposes [18, 19]. The approximant is valid up to the moment of merger frequency defined by NR simulations in [34]. The latter references quantifies the frequency corresponding to the peak of the waveform's amplitude in term of the tidal polarizability coefficient κ^T_2; the amplitude's peak formally marks the end of the chirp signal from BNS. Although our work focused uniquely on the GW phase evolution, tidal corrections to the amplitude could also be added following [30]. Future research will aim at improving the approximants using more NR data and at including precession effects [35, 36]. Our work also proves that high-precision BNS simulations for GW astronomy (similar to those used for the first BBH detections) are now within reach of current technology.

ACKNOWLEDGMENTS

a. Acknowledgments. It is a pleasure to thank S. Babak, B. Brügmann, A. Buonanno, R. Cotesta, W. Del Pozzo, T. Hinderer, B. Lackey, K. Kawaguchi, A. Nagar, S. Ossokine, M. Pürrer for discussions and comments. We thank A. Nagar and T. Hinderer for providing the EOB waveforms. We are grateful to E. Poisson for suggesting the definition of Eq. (2). S.B. acknowledges support by the European Union's H2020 under ERC Starting Grant, grant agreement no. BinGraSp-714626. W.T. was supported by the National Science Foundation under grant PHY-1305387. Computations were performed on SuperMUC at the LRZ (Munich) under the project number pr48pu, Jureca (Jülich) under the project number HPO21, Stampede (Texas, XSEDE allocation - TG-PHY140019), Marconi (ISCRA-B, under the project number HP10BMAB71), and Marconi (PRACE, proposal number 2016153522).

[1] B. . Abbott *et al.* (Virgo, LIGO Scientific), Phys. Rev. Lett. **116**, 061102 (2016), arXiv:1602.03837 [gr-qc].
[2] B. P. Abbott *et al.* (Virgo, LIGO Scientific), Phys. Rev. Lett. **116**, 241103 (2016), arXiv:1606.04855 [gr-qc].
[3] B. P. Abbott *et al.* (Virgo, LIGO Scientific), (2016), arXiv:1607.07456 [astro-ph.HE].
[4] W. Del Pozzo, T. G. F. Li, M. Agathos, C. V. D. Broeck, and S. Vitale, Phys. Rev. Lett. **111**, 071101 (2013), arXiv:1307.8338 [gr-qc].
[5] B. Paczynski, Astrophys. J. **308**, L43 (1986).
[6] N. Tanvir, A. Levan, A. Fruchter, J. Hjorth, K. Wiersema, *et al.*, Nature **500**, 547 (2013), arXiv:1306.4971 [astro-ph.HE].
[7] S. Bernuzzi, A. Nagar, T. Dietrich, and T. Damour, Phys.Rev.Lett. **114**, 161103 (2015), arXiv:1412.4553 [gr-qc].
[8] T. Hinderer *et al.*, (2016), arXiv:1602.00599 [gr-qc].
[9] A. Buonanno and T. Damour, Phys. Rev. **D59**, 084006 (1999), arXiv:gr-qc/9811091.
[10] T. Damour and A. Nagar, Phys. Rev. **D81**, 084016 (2010), arXiv:0911.5041 [gr-qc].
[11] B. D. Lackey, S. Bernuzzi, C. R. Galley, J. Meidam, and C. Van Den Broeck, (2016), arXiv:1610.04742 [gr-qc].
[12] S. Bernuzzi, T. Dietrich, W. Tichy, and B. Brügmann, Phys.Rev. **D89**, 104021 (2014), arXiv:1311.4443 [gr-qc].
[13] K. Hotokezaka, K. Kyutoku, H. Okawa, and M. Shibata, Phys. Rev. **D91**, 064060 (2015), arXiv:1502.03457 [gr-qc].
[14] T. Dietrich and T. Hinderer, (2017), arXiv:1702.02053 [gr-qc].
[15] B. D. Lackey, K. Kyutoku, M. Shibata, P. R. Brady, and J. L. Friedman, Phys.Rev. **D89**, 043009 (2014), arXiv:1303.6298 [gr-qc].
[16] K. Barkett *et al.*, Phys. Rev. **D93**, 044064 (2016), arXiv:1509.05782 [gr-qc].
[17] S. Bernuzzi, A. Nagar, M. Thierfelder, and B. Brügmann, Phys.Rev. **D86**, 044030 (2012), arXiv:1205.3403 [gr-qc].
[18] M. Favata, Phys.Rev.Lett. **112**, 101101 (2014), arXiv:1310.8288 [gr-qc].
[19] L. Wade, J. D. E. Creighton, E. Ochsner, B. D. Lackey, B. F. Farr, *et al.*, (2014), arXiv:1402.5156 [gr-qc].
[20] S. Khan, S. Husa, M. Hannam, F. Ohme, M. Prrer, X. Jimnez Forteza, and A. Boh, Phys. Rev. **D93**, 044007 (2016), arXiv:1508.07253 [gr-qc].
[21] J. S. Read, B. D. Lackey, B. J. Owen, and J. L. Friedman, Phys. Rev. **D79**, 124032 (2009), arXiv:0812.2163 [astro-ph].
[22] W. Tichy, Phys. Rev. D **86**, 064024 (2012), arXiv:1209.5336 [gr-qc].
[23] M. Thierfelder, S. Bernuzzi, and B. Brügmann, Phys.Rev. **D84**, 044012 (2011), arXiv:1104.4751 [gr-qc].
[24] D. Hilditch, S. Bernuzzi, M. Thierfelder, Z. Cao, W. Tichy, *et al.*, Phys. Rev. **D88**, 084057 (2013), arXiv:1212.2901 [gr-qc].
[25] S. Bernuzzi and T. Dietrich, Phys. Rev. **D94**, 064062 (2016), arXiv:1604.07999 [gr-qc].
[26] T. Dietrich, S. Bernuzzi, and W. Tichy, Supplementary material (2017).
[27] T. Dietrich, N. Moldenhauer, N. K. Johnson-McDaniel, S. Bernuzzi, C. M. Markakis, B. Bruegmann, and W. Tichy, Phys. Rev. **D92**, 124007 (2015), arXiv:1507.07100 [gr-qc].
[28] L. Blanchet, Living Rev. Relativity **17**, 2 (2014), arXiv:1310.1528 [gr-qc].
[29] T. Dietrich, S. Bernuzzi, M. Ujevic, and W. Tichy, Phys. Rev. **D95**, 044045 (2017), arXiv:1611.07367 [gr-qc].
[30] T. Damour, A. Nagar, and L. Villain, Phys.Rev. **D85**, 123007 (2012), arXiv:1203.4352 [gr-qc].
[31] SpEC - Spectral Einstein Code, `http://www.black-holes.org/SpEC.html`.
[32] A. H. Mroue, M. A. Scheel, B. Szilagyi, H. P. Pfeiffer, M. Boyle, *et al.*, Phys.Rev.Lett. **111**, 241104 (2013), arXiv:1304.6077 [gr-qc].
[33] A. Nagar, T. Damour, C. Reisswig, and D. Pollney, (2015), arXiv:1506.08457 [gr-qc].
[34] S. Bernuzzi, A. Nagar, S. Balmelli, T. Dietrich, and M. Ujevic, Phys.Rev.Lett. **112**, 201101 (2014), arXiv:1402.6244 [gr-qc].
[35] K. Chatziioannou, A. Klein, N. Yunes, and N. Cornish, (2013), arXiv:1307.4418 [gr-qc].
[36] M. Hannam, P. Schmidt, A. Boh, L. Haegel, S. Husa, F. Ohme, G. Pratten, and M. Prrer, Phys. Rev. Lett. **113**, 151101 (2014), arXiv:1308.3271 [gr-qc].